BOLETIN DE LA SOCIEDAD ESPAÑOLA DE
Cerámica y Vidrio
www.elsevier.es/bsecv

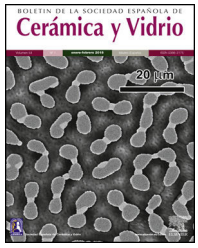

Influence of nanosilica in the chloride binding capacity of sustainables ground blast furnace slag and metakaolin

Alberto Isaac Ruiz, Miguel Ángel de la Rubia, Amparo Moragues, Encarnación Reyes*

Department of Civil Engineering: Construction, School of Civil Engineering, Technical University of Madrid, C/ Profesor Aranguren s/n, 28040 Madrid, Spain

ARTICLE INFO

Article history:
Received 28 July 2023
Accepted 28 September 2023
Available online 2 November 2023

Keywords:
Metakaolin
Ground blast furnace slag
Nanosilica
Chlorides durability
Sustainability

ABSTRACT

This work investigates the chloride binding capacity combine of two sustainable pozzolanic additions such as granulated blast furnace slag (G) and metakaolin (M) used in cement to decrease its carbon footprint. They are also combined with two nanosilicas with different specific surface area (O and A). Blends of alone M or G and with nanosilica are mixed in water with $Ca(OH)_2$ and chloride (C) to compare chloride binding capacity of both in presence or not of nanosilica. Blends are analysed by XRD, FTIR, DTA–TG and chloride binding capacity is determined too by potentriometric titration with $AgNO_3$. The addition of chlorides to both pozzolanic M and G indicates that M shows higher chloride binding capacity than G although very similar Friedel's salt formation, indicating a higher physisorbed chlorides contain. Chlorides addition meaningfully replaces carbonates in carboaluminates phases to form Friedel's salt, being this exchange higher for samples with M than for G blends. The combination of experimental techniques used in this study have shown that the effect of nanosilica addition to samples with M and G show an opposite effect in Friedel's salt formation, increasing for samples with G and decreasing for samples that contain M.

Influencia de la nanosílice en la capacidad de combinación de cloruros de la escoria de alto horno molida y metacaolín sostenibles

Palabras clave:
Metacaolín
Escoria de alto molida
Nanosílice
Durabilidad frente a cloruros
Sostenibilidad

RESUMEN

Este trabajo investiga la capacidad de combinación de cloruros de dos adiciones puzolánicas sostenibles, como son la escoria granulada de alto horno (G) y el metacaolín (M), que se utilizan en el cemento para reducir su huella de carbono. Estas se combinan con dos nanosílices de diferente superficie específica (O y A). Mezclas de M y G solas y con nanosílice se mezclan en agua con $Ca(OH)_2$ (CH) y cloruro Cl^- (C) para comparar la capacidad combinación del cloruro. Las mezclas se analizan mediante DRX, FTIR y ATD-TG, y la capacidad de unión

* *Corresponding author.*
E-mail address: miguelangel.rubia@upm.es (M.Á. de la Rubia).
https://doi.org/10.1016/j.bsecv.2023.09.002

de cloruro también se determina mediante tritación potenciométrica con $AgNO_3$. La adición de cloruros a las composiciones con M o G sin nanosílice indica que el M muestra una mayor capacidad de combinación de cloruros que la G, siendo la formación de sal de Friedel muy similar, lo cual indica un mayor contenido de cloruros fisisorbidos. La adición de cloruros reemplaza significativamente a los carbonatos de los carboaluminatos para formar la sal de Friedel, siendo este intercambio mayor para las muestras con M que para las mezclas con G. La combinación de las técnicas experimentales utilizadas en este estudio ha demostrado que el efecto de la adición de nanosílice a las mezclas con M y G muestra un efecto opuesto en la formación de la sal de Friedel, aumentando para las muestras con G y disminuyendo para las que contienen M.

Introduction

Up to the present Portland cement (PC) has been the most widely used binder in civil engineering construction, owing to its good price-performance ratio. However, The great current environmental crisis has meant that the use of PC is being increasingly questioned due to the high CO_2 emissions generated throughout its Lifecycle (LC) [1]. The carbon footprint is a key indicator to control the emissions of any material produced and its reduction is a requirement for the implementation of more sustainable materials. Besides that, it is essential that the concepts of service life and durability go hand in hand with the design of new steel reinforced concrete structures, which could result in a significant saving in the cost of maintenance and a positive impact on their LC [2–4], thus contributing to sustainability.

One of the most recurrent options in the PC industry to reduce the Carbon Footprint is based on extending its Service Life. This is achieved by improving mechanical properties and durability against the attack of aggressive agents, thus amortising the high cost of the construction, repair and maintenance work [3,4]. Resistance to corrosion stands out among the main aspects studied [5,6] regarding the preservation of physical and mechanical properties in PC, and so its ability to protect steel against corrosion. It is also one of the most worrying issues because of the considerable economic impact that steel corrosion in reinforced concrete structures represents.

Corrosion of steel reinforcement leads to the loss of structural integrity and the serviceability of reinforced concrete [7,8]. The penetration of chloride ions from de-icing salt or seawater represents the most important contribution to the degradation of reinforced concrete. These salts cause depassivation of the steel reinforcement when the chloride concentration exceeds a certain threshold level [5,9,10].

From the literature [5,10–13], the chloride ions in the diffuse layer of the calcium silicate phase (C—S—H) are chemically bound to the formation of Friedel's salt ($3CaO–Al_2O_3–CaCl_2–10H_2O$) or Kuzel's salt ($3CaO–Al_2O_3–1/2CaCl_2 1/2CaSO_4–11H_2O$). Both salts usually form the bound chloride in exposed concrete. As they are chemically combined, they are not likely to corrode the reinforcement. The remaining chloride ions may be present in as free chloride in the pore solution, which could represent the problem with corrosion.

The most commonly used method to evaluate the resistance of concrete to chloride penetration is the diffusion coefficient. This method is based on total chloride profiles (% chloride per depth of penetration), which are directly related to the pore structure [13,14].

Regarding this, previous studies state that Portland cement hydration generates a physical constraint on the rate of chloride ingress [5,15–19]. Another recent study [20] has extensively demonstrated that chloride ions easily penetrate the C—S—H diffusion layer. This suggests a great need to extend the current knowledge on chloride binding mechanisms and to evaluate their persistence in concrete as well as the resistance of the concrete to penetration. The use of supplementary cementitious materials (SMC) has emerged as a possible solution to improve resistance to chloride penetration thus improving durability while reducing the consumption of portland cilinker, thus contributing to sustainability in both ways. These include a wide range of materials such as metakaolin (M), silica fume (SF), ground blast furnace slag (G), fly ash (FA) and materials of pozzolanic and alumina-rich origin [12,17–19,21,22].

Furthermore, some of these are industrial wastes that would otherwise be discarded, ending the life cycle of the production process. Actually, SMCs have proven to be functional materials, favouring the reduction of the carbon footprint in some cases and increasing durability against aggressive agents [2,3,7,8,23]. Previous studies [10,12,20,24] show a positive effect associated with microstructural densification of the Portland cement matrix by the use of micro- and nano-materials. It has been observed that alumina-rich ($2SiO_2–Al_2O_3$) SMCs cooperate in chloride binding through Friedel's Salt formation. However, very few studies focus on chloride adsorption in the diffuse layer of the C—S—H phase, although such physical binding is described in detail in several studies for synthetic C—S—H phases [25–29] hydrated Ca_3SiO_5 (C_3S) [30], Portland cement [31], and Silica fume-lime mixtures [32–34]. This is probably attributable to the fact that, given the marked heterogeneity of the C—S—H phase in composition and structure, it

is much more complicated to identify physical Cl^- bonds, which prevents the establishment of a reliable approach to assess the contribution of alumina-rich SMCs in particular to total chloride bonding that includes chloride adsorption.

Metakaolin (M) is the product of the heat treatment of kaolin clay between 600 and 800 °C. It has a high content of amorphous silica and alumina [35,36]. Dinkar et al. [37] evaluated the optimum replacement rate of Portland cement by metakaolin, observing a decrease in fluid permeability, which minimised the absorption of aggressive agents such as chlorides and atmospheric CO_2, with an addition of 10% M by weight [38,39]. Ground blast furnace slag (G) is a non-metallic residue from the steel industry derived from the indirect reduction of iron at temperatures above 1500 °C. This residue is granulated by a blast cooling process or by rapid immersion in water. The addition of granulated slag grindings as a binder in a cementitious paste leads to a decrease in the chloride diffusion coefficient through the reinforced concrete, making it more difficult for Cl^- to reach the steel of the structure and increasing its corrosion resistance [22,40–43]. Substitution ratios are usually high, in the range of 30–70%, significantly reducing the use of Portland clinker.

Nanosilica usually has a high level of pozzolanic reactivity and very fast kinetics. It densifies mortars at the microstructural level as C—S—H can do, which may improve mechanical properties and especially durability [33,34]. It alters the rheology of cement-base materials by increasing the C—S—H content and easily modifies the hydrated calcium silicate chains compared to Portland cement or other SMCs [24,44]. It strongly influences the fixation of free chlorides but very little the formation of Friedel's salt [20,21]. Studies carried out with ternary mixtures of Portland cement with M and nanosilica (10% and 3% respectively) as Andrade da Silica et al. [45] showed an increase in compressive strength in the order of 30% and an overall improvement in chloride ion penetration resistance. Moreover, García et al. [23,46] evaluated the capacity of pozzolanic additions with NS in aqueous phase excluding Portland cement, showing that M favours the chemical binding capacity of the chloride ion through the formation of Friedel's salt. The clear tendency of such mixtures to form C—A—S—H was also demonstrated [13,36,44,47–51]. Also, the use of nano additions has been shown to be effective in improving the mechanical properties of Portland cement base materials.

The aim of the present work is to compare the performance of different SMCs in the aqueous phase with respect to their chloride binding capacity. Specifically, M, nanosilicas and G. Two classes of nanosilicas with different specific surface area, combined separately with M and G, have been evaluated. The absence of Portland cement will allow to observe the interaction of these materials and evaluate their ability to form chloride bonds without interference. Therefore, the possible synergistic, additive or antagonistic effect of these materials will be determined. The data obtained should provide clear and detailed information on the viability of each SMC as a component in the design of more sustainable cement-base materials, resistant to environmental aggressions with lower consumption of portland clinker and a longer service life.

Table 1 – Physical characteristics of materials.

Material	Particle size, nm	Surface specific area, m^2/g
Metamax (M)	~1300	12.56
Ground blast furnace slag (G)	~6160	1.77
Nanosilica OX50 (O)	~40	50 ± 15
Nanosilica A200 (A)	~12	200 ± 25

Materials and methods

Materials

The metakaolin (M) used is of the brand METAMAX. It exhibits high pozzolanic reactivity and was produced from high purity kaolin clay through a 750 °C calcination process. The granulated blast furnace slag (G) is a residue obtained in the indirect reduction of iron in a blast furnace close to 1500 °C to obtain steel. The G used in this study comes from a steel work in Northern Spain. On the other hand, two pyrogenic hydrophilic nanosilicas with different specific surface, AEROSIL 50 (OX50) and 200 (A200) from Evonik Industries, were selected for this study. Additionally, calcium hydroxide (CH) with a purity > 95.0 wt.% from SCHARLAB and sodium chloride from LABQUEM with a purity ≥ 99.9 wt.% were used. According to nomenclature used in abstract and introduction, in the following text and figures of the manuscript metakaolin will be abbreviated as M, ground blast furnace slag as G, nanosilica OX-50 and A200 as O and A respectively. Blends containing chloride are indicated with a letter C. The measurement of the specific surface area (BET) was carried out using the nitrogen adsorption technique at 77 K with the Quantachrome Monosorb Surface Area Analyser MS-13. Values are shown in Table 1 as well as the mean particle size.

A wavelength dispersive X-ray fluorescence spectrometer (MAGI X -PANALYTICAL) was used to determine the chemical composition of metakaolin and pulverised blast furnace slag. Table 2 shows the chemical composition of these materials and the NS data provided by the manufacturer.

Paste design and suspension preparation

The M/A-O weight ratio of 4:1 [23,52] was established for the design of the pastes for a total of 12 combinations under the prior assumption that only 50% of the mixtures would include sodium chloride (NaCl), as shown in Table 3, where the abbreviated notation for each sample is also collected. In order to keep the Al/Si ratio in M and A/O constant, the weight of G was estimated for all additions to match the same in accordance with their chemical composition (Table 2). To ensure comparability and reproducibility of the results obtained, it is vital to keep this ratio under control since Al_2O_3 is involved in the formation of chemically combined chlorides [11,47,49].

Portland cement is not considered in the design in order to avoid its contribution to the generation of C—S—H and C—A—S—H gels by its hydration such as the formation of Friedel's salt by combination of chlorides. To simulate the marine environment, the molar concentration of Cl^- was set at 0.5 M [10,21,31,46], similar to that of seawater. The molar

Table 2 – Chemical analysis of materials.

Chemical analysis	CaO	Fe_2O_3	K_2O	MgO	Na_2O	SiO_2	TiO_2	Al_2O_3	P_2O_5	MnO	ZnO	SO_3	LOI
Metakaolin (M)		0.41	0.12		0.16	52.4	1.83	44.9	0.08				0.1
Ground blast furnace slag (G)	42.7	0.34	0.43	7.8	0.47	34.1	0.58	10.5	0.04	0.14	0.6	2	0.34
Nanosilica (O)						99.8							0.01
Nanosilica (A)						99.8							0.01

Table 3 – Composition of mixtures prepared.

Mixture dosage	Mixtures acronyms/ dosage (g)	O	A	M	G	CH	C	Distilled water
Metakaolin	M	–	–	5	–	1.6	–	250
Ground blast furnace slag	G	–	–	–	21.38	1.6	–	250
Metakaolin + Cl^-	MC	–	–	5	–	1.6	7.3125	250
Ground blast furnace slag + Cl^-	GC	–	–	–	21.38	1.6	7.3125	250
Metakaolin + nanosilica OX50	MO	1.25	–	5	–	1.6	–	250
Ground blast furnace slag + nanosilica OX50	GO	1.25	–	–	21.38	1.6	–	250
Metakaolin + nanosilica OX50 + Cl^-	MOC	1.25	–	5	–	1.6	7.3125	250
Ground blast furnace slag + nanosilica A200 + Cl^-	GAC	1.25	–	–	21.38	1.6	7.3125	250
Metakaolin + nanosilica A200	MA	–	1.25	5	–	1.6	–	250
Ground blast furnace slag + nanosilica A200	GA	–	1.25	–	21.38	1.6	–	250
Metakaolin + nanosilica A200 + Cl^-	MAC	–	1.25	5	–	1.6	7.3125	250
Ground blast furnace slag + nanosilica A200 + Cl^-	GAC	–	1.25	–	21.38	1.6	7.3125	250

solubility of $Ca(OH)_2$ in water at 25 °C is 1.6 g/l, guaranteeing that aqueous suspensions prepared are supersaturated.

The suspension preparation process was as follows; weighing of the dry powdered materials and distilled water, followed by a 7-day period of constant stirring to ensure calcium fixation [25,28,30], filtering process for the six Cl^- free samples, addition of NaCl to the remaining solutions and constant stirring for 21 days to ensure maximum Cl^- combination, finally the six samples with Cl^- were also filtered. The paste resulting from the filtering process was treated at 100 °C for 24 h in a drying oven, obtaining as a result a dry powder sample of each mixture.

Characterization of the mixtures

The resulting powder of each mixture was chemically characterised by DTA–TG, FTIR, XDR and, additionally, in the case of samples with Cl^-, the content of free and total chlorides was quantified by potentiometric titration with $AgNO_3$. Differential thermal analysis and thermogravimetry (DTA–TG) of the powders was carried out under a temperature range between 25 and 1100 °C, with a heating rate of 10 °C/min in N_2 atmosphere and alumina crucibles. A TGA-LABSYS evo provided by SETARAM Instrumentation was used.

The chemical composition analysis was carried out by X-ray diffraction (XRD) using a Bruker D8 Advance diffractometer using monochromatic Cu Ka radiation with a wavelength $l = 1541$ Å. A high-speed detector (Lynxeye) between Bragg angles 5–60° θ and a step size of 0.02° θ were used.

The identification of the crystalline phases was performed by comparison with the Joint Committee on Powder Diffraction Standards (JCPDS) guidelines. FTIR analysis of the samples prepared by the KBr Pellet Method was performed with a Perkin Elmer Spectrum 100 Spectrophotometer, with a wavenumber range between 400 and 4000 cm^{-1}.

The determination of the chloride content was carried out in two phases: Phase 1 to determine the free chlorides and Phase 2 to determine the total chlorides. The materials used for Phase 1 were: 150 ml beakers, a magnetic stirrer, a 100 ml volumetric flask, glass funnel with 1410 filter paper and reagents were used in the first phase. First of all, 1.0010 ± g was added to each beaker with 10 ml of distilled water and stirred constantly for 3 min. This was left to filter for a while in the volumetric flask, 2 ml concentrated HNO_3 (nitric acid) was added and distilled water was added up to the volumetric mark. The contents are poured into the previously cleaned beakers and a pH check is made with 0.5 ml sodium acetate $NaC_2H_3O_2$ and 20 ml acetic acid $C_2H_4O_2$ and finally the free Cl^- content is titrated using a Metrohm measuring instrument. This incorporates 0.025 M $AgNO_3$ at a constant rate and the free Cl^- is determined.

The materials used for Phase 2 were: 250 ml beakers, glass clocks, stirrers and magnetic heating plates were used for the second phase. The procedure followed in this phase began adding 1.0010 ± g to each beaker with 100 ml of distilled water. This mixture was stirred constantly and left to boil for 3 min. Then, total Cl^- is titrated using 0.050 M $AgNO_3$. Once the % of free and total chlorides present in the samples is known, the % of combined Cl^-, which includes physically and chemically bound Cl^-, can be estimated by difference. The first ones are those found directly in gels and the second ones are found after Friedel's salt formation.

Results and discussion

XRD diffraction

The diffraction patterns of the samples are shown in Fig. 1. As it is observed in the diffractograms recorded for the G and M, there is an amorphous halo between 20 and 35° 2θ, as a result of the amorphization process to obtain M according

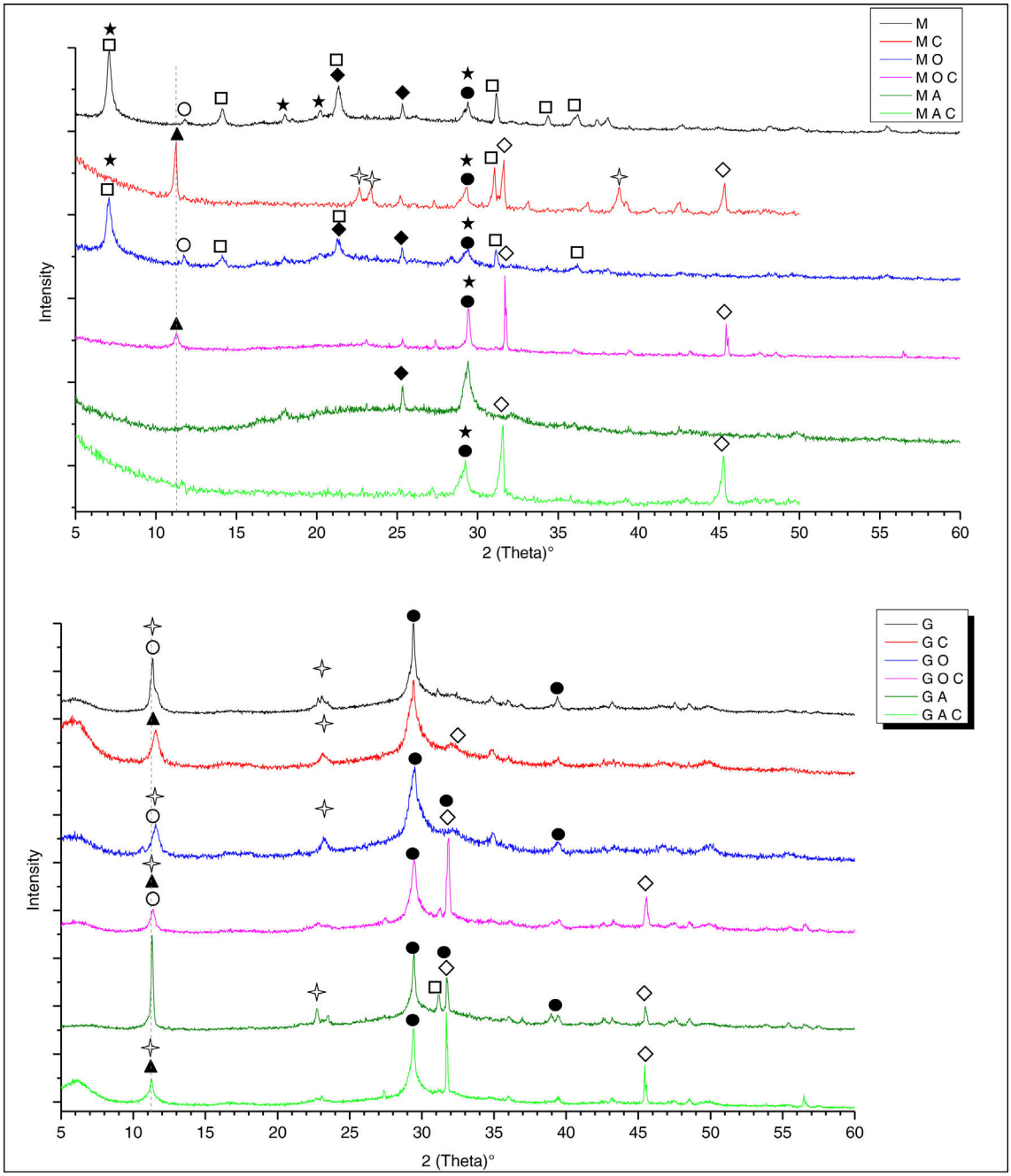

Fig. 1 – X-ray diffraction of mixtures, • calcite $CaCO_3$, ♦ SiO_2 quartz, ○ hydrated hemicarboaluminate $C_4Ac_{0.5}H_{11.5}$, □ stratlingite C_2ASH8, * beidellite AS_4H, Friedel's salt, halite, hydrotalcite $Mg_6Al_2(CO_3)(OH)_{16}{\cdot}4H_2O$.

to the thermal treatment of kaolin between 700 and 800 °C and the formation of G cooling from the very high temperature (1600 °C) used in a blast furnace in obtaining steel. For M samples the halo amorphous is higher in samples with the addition of nanosilica.

Certainly, a characteristic signal shape can be observed for each addition. These signals are wider for G, showing an intensity similar to that of a relatively amorphous structure. This is in contrast to M where a signal shape more similar to a crystalline phase is observed in the MC.

The G samples show signal overlap between 11.2 and 11.5° 2θ, and therefore the identification of products in this band becomes complicated. This zone may correspond to several hydration products, such as Friedel's salt formation or similar. In samples G, GO and GA this bands could be associated with the formation of C_4ACC-OH carbo-aluminates [53,54]. However, the presence of 7.8% MgO in the chemical composition of G would promote the formation of Hydrocalcite Mg_6–$Al_2(OH)_{16}$–(CO_3)–$4H_2O$ [55–57]. The shape of the signal could be distinguished for each addition, for example for G the signals are wider showing an intensity similar to a more amorphous than crystalline structure than the opposite case for M in the MC a signal more common to a crystalline phase is observed.

Stranglinite mineral, 6.5° 2θ, can be identified in samples with M as well as a constant formation of Friedel's salt at 11.20° 2θ [11,13,47], which can be observed along the dashed grey line pattern, with the exception of sample MAC where both the modification of hydration products and formation of Friedel's salt are associated to the presence of nanosilica A. This is most likely due to nanosilica A preventing or limiting the access of M to Cl^-, avoiding the formation of Friedel's salt [46] and also to calcium avoiding the evolution of the formation of hydration products.

The presence of halite (NaCl) is observed at 31.9 and 45.5° 2θ due to the incorporation of this salt in the aqueous solutions [31].

Regarding the presence of C—S—H and C—A—S—H gels as hydration products, two peaks are identified at 29.3 and 32.6° 2θ which presumably correspond to the incorporation of Al in these gels. It is however not possible to quantify them, due to the presence of overlapping calcite in these signal bands [58]. Kapeluszna indeed locates the C—S—H gel in that area [59] although presenting very intense and sharp peaks which differ from those of Fig. 1. Additionally, Kapeluszna [59] describes the hexagonal AFm phases C_2AH_8 and C_2AH_6, resulting from the dehydration of C_2AH_8 in synthetic gels with an Al/Si ratio of 0.125 and 0.2.

The author locates these phases at 10.2, 20.6 and 36.0° 2θ but they could not be identified in this particular study, as can be seen in Fig. 1. The reason is attributed to the type of Silica and Aluminium contained in the M and G, which have been combined with each type of nanosilica. The Al/Si molar ratios established in this study, ranging from 0.30 to 0.97, is very high compared to that described by Kapeluszna, which uses $Na_2Si_3O_7$ as the silica source and $Al(NO_3)_3$ as the aluminium source.

The addition of nanosilica, especially A, promotes the generation of structures with a stronger crystalline character, as can be seen in 29.5 and 11.2° 2θ.

For samples with metakaolin, the addition of chlorides favours the samples carbonation.

Samples with slag both with and without chlorides have a much greater tendency to carbonate than sample with metakaolin.

Finally, from the obtained results, it can be concluded that the addition of Cl^- encourages the formation of aluminosilicates in both types of mixes, with a stronger tendency in the case of samples with slag. However, there is a problem present that prevents asserting the reason for the calcite signal fitting to the C—S—H and C—A—S—H signal.

FTIR analysis

The FTIR characterisation results of the twelve pastes were obtained. The vibration bands appearing in the FTIR spectra are the same for the gels from aluminate hydration and the gels from Silicate hydration [59]. There is concurrence with characteristic signals of C—S—H, C—A—S—H and CAH gels in the results for M pastes and concurrence also with characteristic signals for silico-aluminate and silicate hydrated G pastes previously described in the literature [59,60]. According to these previous works, certain vibrational and binding modes are assigned for C—S—H, C—A—S—H, CAH and Cl^- combinations. The high and low frequency infrared results can be seen in Fig. 2.

Around the bands 965 and 962 cm^{-1} a signal is found which can be associated to the primary C—S—H gel generated by the Si—O stretching vibration. For M samples, the FTIR spectrum varies and shows an intense and broad band with a signal at 1070 cm^{-1}. This signal indicates the substitution of SiO_4 tetrahedra by tetrahedral Al (AlO_4) in the chains of the Dreikeiten Structure polymerising the 1D to 2D and 3D structure by bridging [61] Q_{2b} or Q_3.

The signals appearing at around 495–1070 cm^{-1}, typical of Si—O—Si asymmetric stretching vibrations, may be attributed to polymerised silica.

For samples with metakaolin, the splitting peak located at 530 and 585 cm^{-1} corresponds to the stretching vibrations of Al—OH bonds of $Al(OH)_6$ octahedra corresponding to some unreacted metakaolin while the peak located at 788 cm^{-1} corresponds to its bending vibration, which are attributed to the Friedel's salt. Primary C—S—H gel band appears around 970 cm^{-1} due to Si—O stretching vibration and, in addition, a shift takes places from 970 to 1050–1150 cm^{-1} indicating the substitution of Si by Al, forming C—A—S—H gel with AlO_4 tetrahedra joined to SiO_4 tetrahedra. The incorporation of aluminium to C—S—H gel to form C—(A)—S—H gel occurs mainly in tetrahedrally coordinated Al (IV) in bridging tetrahedra Q_{2b} and sometimes in bridging tetrahedra Q_3 [61]. The presence of the peaks at 530 cm^{-1} corresponds to the Al—O—Al vibrations, that can corresponds to AlO_4, AlO_5 and AlO_6 units, according to literature [59,62]. However at 1070 cm^{-1} appears a wide and strong peak, corresponding to the asymmetric stretching vibration of Si—O—Si of polymerised silica.

The 3641 cm^{-1} signal is associated with the vibration of the OH groups of $Ca(OH)_2$ present in the C—S—H gel as observed in the literature [59,62,63], however, due to the presence of Al, this structure tends to transform into C—A—S—H and so it should be scarcely present. This behaviour is most commonly observed in experiments with Ca/Si < 1 ratios [58,59], however some authors point out the possibility of weak observation of the 3646 cm^{-1} signal with ≥1.7 ratios.

As observed in previous works [47,59,60] bands 422 and 525 cm^{-1} correspond to the O—Al—O and Al—O—Al (AlO_4, AlO_5, AlO_6) bending vibrations and are associated respectively with the C_2AH_8 ($2CaO–Al_2O_3–6H_2O$) and the dehydration product C_2AH_6 ($2CaO–Al_2O_3–6H_2O$). Both signals can be found in samples M and G. Kapeluszna [59] states that this band signal is, in any case, not particularly visible or very weak, as is the case in the MO, MA, MOC, MAC and almost all G samples except for GC. The signal observed at 530, 564–600 cm^{-1} can be attributed to two bands or splitting peaks associated to the stretching vibrations of the Al—OH bonds of the $Al(OH)_6$ octahedra related to unreacted Al from M and G.

Another point to note is that the signal located between 788 and 800 cm^{-1}, attributed to Friedel's salt (3CaAlCaClH) as a crystal structure and chemical combination of Cl^-. For samples with M, the addition of nanosilica decrease the presence of Friedel's salt and for G only in the sample without nanosilica is clearly identify Friedel's salt. Therefore by FTIR analysis FS can only be confirmed in the MC, MOC and GC samples. This can be due to that samples with G, which results in a more intense silicate or silico-aluminate formation activity in the

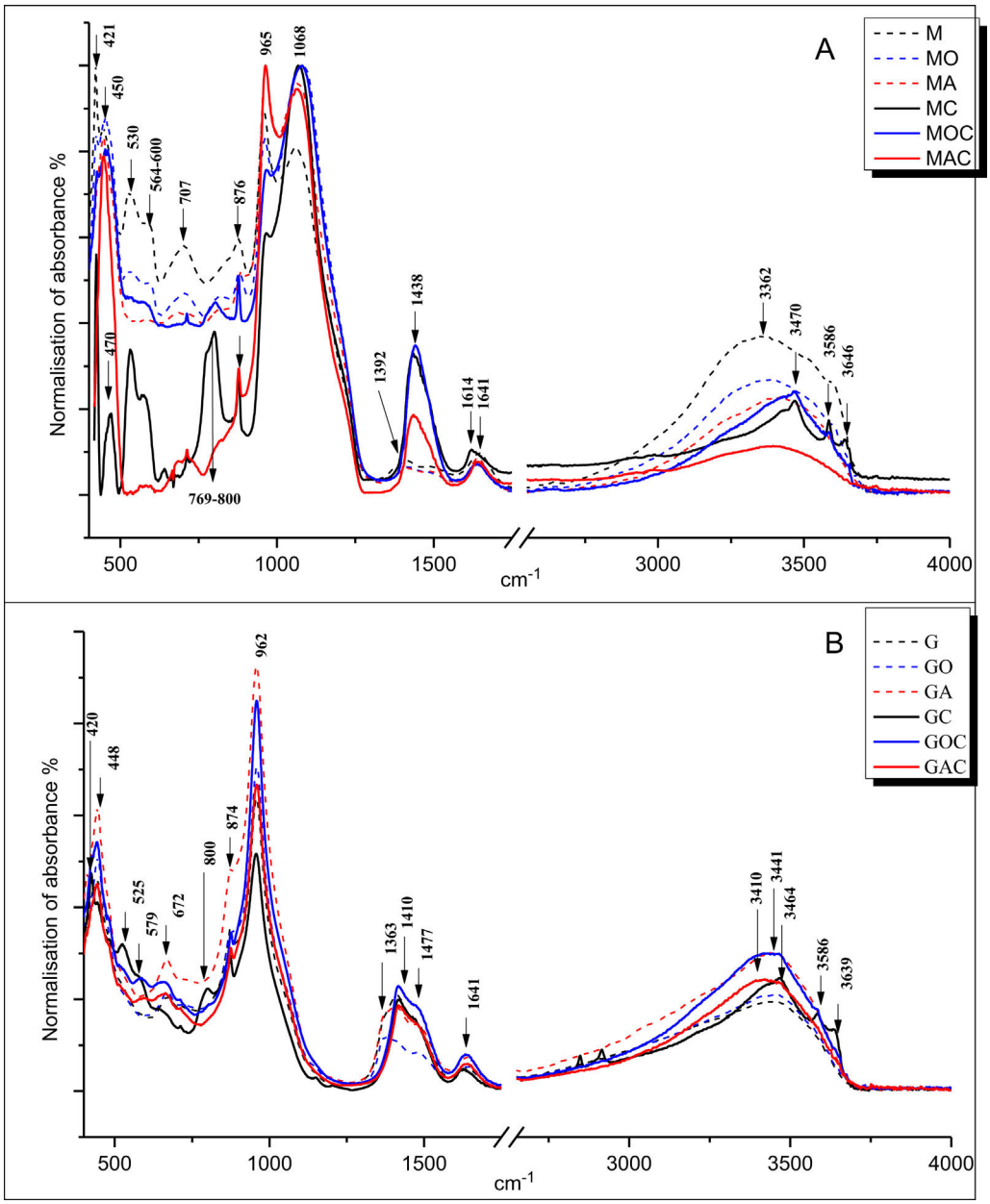

Fig. 2 – Low and high frequency FTIR analysis of the different mixtures prepared for 7 days and 21 days.

presence of Cl^-, also forming Hydrotalcite, hydration product in G blends with high capacity to binding chloride ions. As an atypical situation, in the specific case of MOC samples, the addition of nano-silica seems not to be an impediment for Friedel's salt formation, although the signal intensity is clearly lower. The FTIR analysis then confirms the previous XRD observations by asserting that there are overlaps around 11.2 and 11.6° 2θ.

When observing in detail in Fig. 2b, two signals within 1420–1450 cm^{-1} and 876–880 cm^{-1} are distinguished, belonging to υ_2 of the C—O bond of the CO32-b carbonate. These are non-stable areas of Al—O bonds [53,64] associated with the carbonation of the gels in a natural way, which are enhanced in the presence of Cl^-, as in the case of MC, MOC, MAC and all G, except for the GOC samples where the feature is observed with less intensity.

Another issue to note is the presence of water at 1645 cm^{-1}. Kapeluszna [59] determines that its presence corresponds to the O—H bending vibration whereas the 3500 cm^{-1} signal corresponds to the O—H stretching vibration. These signals are somewhat diffuse and indicate weakly crystalline or amorphous phases which may confirm the presence of some hydrated aluminosilicates.

Finally, it should be noted that the M combinations are more likely than the G combinations to polymerise the Si present in the solution. As a direct consequence, the probability of forming C—A—S—H gels with M due to the incorporation of AlO_4 in its structure is higher. However, it should be noted

that this gel formation potential may vary depending on the morphology and structure of the Al present in the M.

These statements are in agreement with the work of Kapeluszna et al. [59] and can be verified by the data in Fig. 2. This shows that the origin and type of materials can give rise to hydration products, Cl^- combination and modifications of these after incorporation into the PC.

Thermal analysis (DTA–TG)

The TG test shows the mass loss in time and temperature in a decreasing trend. Therefore, in order to determine these changes, the thermos-gravimetric derivative DTG is performed, allowing a better resolution on the TG-plot. The DTG results are quantitatively analysed by studying three typical endothermic contribution zones corresponding to hydration reactions.

For the first zone, the dehydration of C—S—H or C—(A)—S—H gels such as hydrated calcium silicates and hydrated calcium alumino-silicates is analysed according to the Al content and is set at the interval from 105 to 250 °C. The second zone, is between 250 and 400 °C corresponding mass loss for Friedel's salt water [21] according to others authors [5,13] describe thermal signals where the formation of synthesised Friedel's salt appears and can be overlapped with other hydration products delimited by the 230–400 °C zone as an extended range [13]. In this thermal range takes place the dehydroxilation of the main sheets in Friedel salt. Peak between 400 and 550 °C corresponding to the dehydration of portlandite [65]. The last zone, at higher temperatures than 550 °C, corresponds to the carbonation of the gel and portlandite such the possible presence of another carbonates as raw materials, and is located between 550 and 1100 °C [65]. According to literature, carbonated portlandite corresponds to 41 wt.% of total carbonates. In this respect it should be noted that potential Friedel's salt dehydration coincides in the first zone with typical signals at 110 °C, 180 °C and approximately 330 °C with overlapping signals from other types of hydration products such as carbo-aluminates [53]. This weight loss is due to the removal of water molecules in the interlayer space and this process results in a product with reduced crystallinity $3Ca(OH)_2$—$2Al(OH)_3{\cdot}CaCl_2$ [13,47]. Although there are discrepancies about the dehydration of Friedel's salt being in the dehydration zone of the gel, clear or split signals have been observed in this experiment between 250 and 400 °C [13,65–69]. Therefore in samples with M and G the quantification at lowest temperature range (105–250 °C) is performed to observe the changes in gel formation in the presence of NS and chlorides for each addition, since at temperature around 135 °C takes place water removal in Friedel's salt. Fig. 3 shows the DTG of the G samples combined with the nanosilica and chlorides and furthermore compares six graphs with and without chlorides plus $Ca(OH)_2$ separated in pairs.

In the specific case of the G samples, a very significant amount of hydration products can be observed in the gel zone at a temperature around 221 °C associated with AFm or carbo-aluminates [54]. Temperatures of 406 °C and 450–550 °C, which can be associated with a $Ca(OH)_2$-like structure, are also interesting, although it could be merely its leaching during the agitation process. The presence of nanosilica produces a narrowing of the carbonation zone compared to sample G. A significant formation of high-temperature carbonates (850–1100 °C) is also observed, which are directly associated with the incorporated Cl^-.

By incorporating Cl^-, which is represented by a red line for each pair of graphs (Fig. 3), the hydration of the G is significantly modified, which apparently leads to an increase in C—S—H or CAH formation between 140 and 150 °C. Contrary to the XRD and FTIR data, the thermal analysis shows a possible formation of Friedel's salt around 340–350 °C.

Table 4 shows the percentage of loss for each G combination and this information agrees with what is observed in Fig. 3. There is a clear tendency to form more gels or hydration products in the 105–250 °C zone when nanosilica is incorporated and a same trend in the rate of carbonate formation. Cl^- addition decreases considerably C—S—H and C—(A)—S—H gels for samples with G with and without nanosilica. C—S—H and C—(A)—S—H gels contain increases regardless of the addition or not of chlorides. In the 250–400 °C temperature range it is not take account the weight losses in samples in absence of chloride since Friedel salt it is not possible to form it. Nanosilica addition to G increases the chemical binding capacity of chlorides of the blends since significantly increases its formation for both nanosilicas. Moreover, according to much higher weight loss between 550 and 1100 °C associated to carbonates, it is really remarkable that added chlorides displace carbonates in carboaluminates phases to form Friedel's salt ($3CaO{\cdot}Al_2O_3{\cdot}CaCl_2{\cdot}10H$) and calcium carbonate. This carbonates are release as CO_2 at higher temperature according to Figs. 3 and 4. This exchange is higher for samples with M than for G ones and supposes an increase in the weight loss associated to carbonates between 2–6 and 5–9 times more for G and M respectively according to Tables 4 and 5. According to literature [67–69], samples carbonation destabilises Friedel's salt and according to this study the chloride addition displace carbonates in carboaluminates to form Friedel's salt. Therefore can be stablished to exist a reversible equilibrium conditioned between the formation of Friedel's salt that chemically combines chlorides or destabilization of this phase by carbonation depending on the exposure to chlorides or carbonation in the environment.

According to Table 5, samples containing M presented a very different behaviour. In this case the experimental results showed that the hydration of the silicoaluminates were more noticeable with respect to the samples with G. In the same way that blends with G and nanosilica, the nanosilica addition to samples with M decreases the gel C—S—H and C—(A)—S—H gels and in a very drastic way in the sample without nanosilica, with a decrease of 50 wt.%. Unlike the samples with blast furnace slag in which the addition of nanosilica increases the gel formation it is important emphasise that in blends with metakaolin when nanosilica is added the C—S—H and C—(A)—S—H gels decreases. It is very important to note that the comparison of the total gel content formed in blends with M and G cannot be carried out because the amount of metakaolin and slag used in the preparation of the different samples has been determined so that the content of alumina, involved in the formation of Friedel's salt is the same being this point the main objective of this research work. For example silica con-

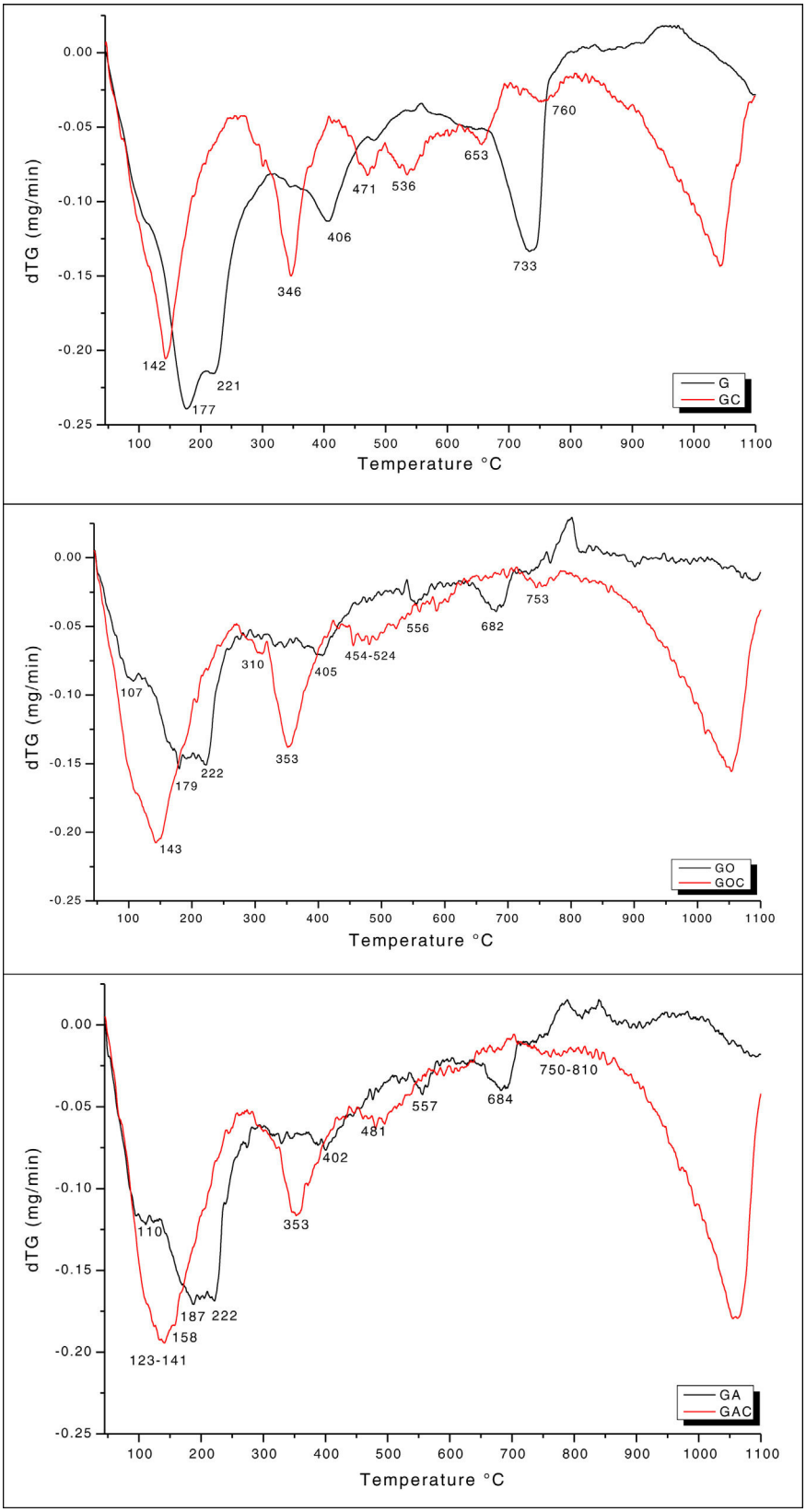

Fig. 3 – DTG thermal analysis of the mixtures prepared with G and NS.

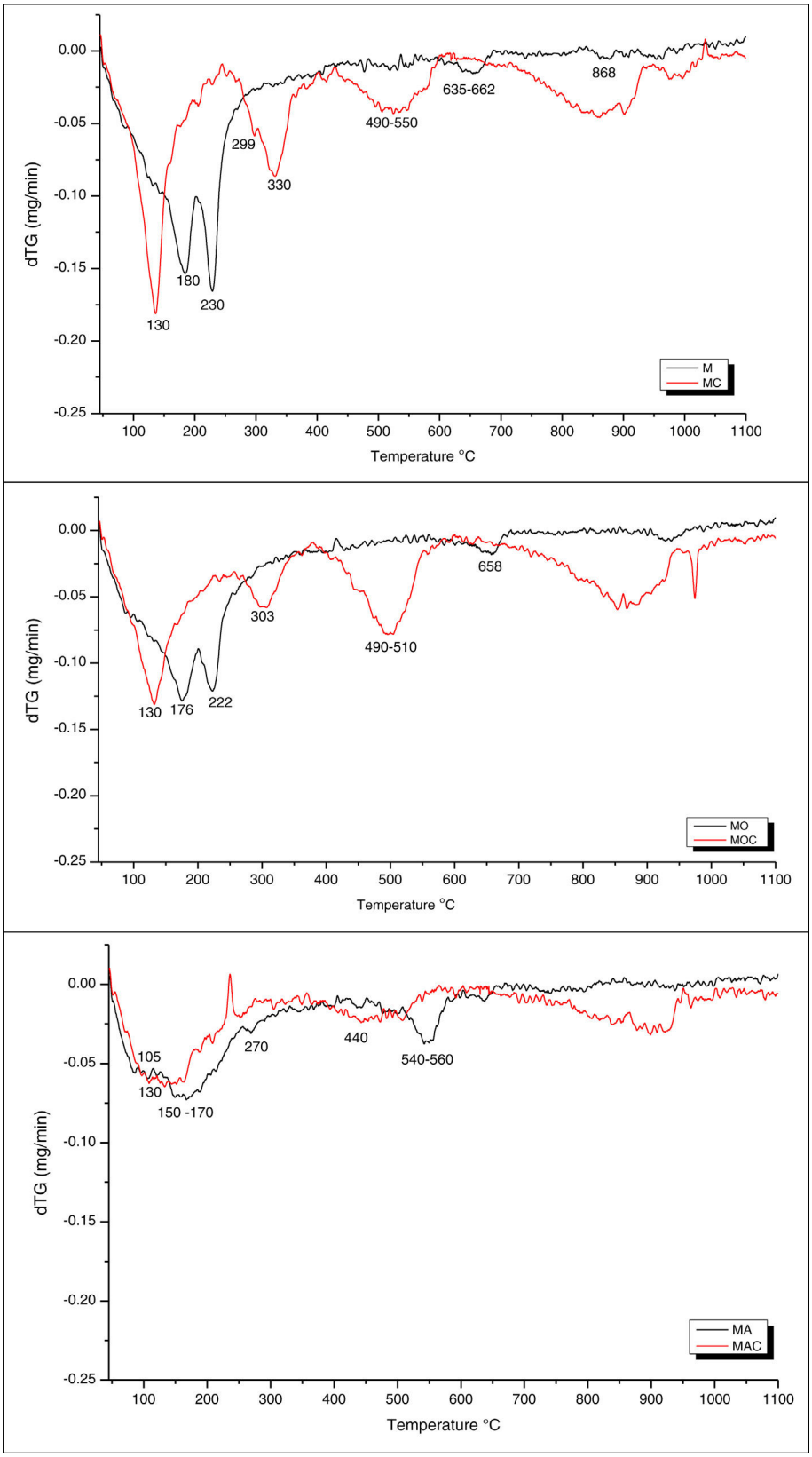

Fig. 4 – Thermal DTG analysis of the mixtures prepared with M and NS.

Table 4 – Weight loss of samples with G in different temperature ranges associated with the three zones for chloride-free and chloride-containing mixtures.

T^e (°C) range/associated weight loss	G% loss	GO% loss	GA% loss	GC% loss	GOC% loss	GAC% loss
105–250/(C—S—H, C—(A)—S—H) gels water	5.79	7.49	7.06	4.01	6.68	6.90
250–400/water in Friedel's salt	–	–	–	3.00	4.24	4.18
400–550/dehydration of portlandite	2.18	2.47	2.49	2.47	2.73	2.88
550–1100/carbonates	3.17	1.93	1.63	7.46	8.99	10.22
(550–1100) × 0.41/carbonated portlandite	1.30	0.79	0.67	3.06	3.68	4.19

Table 5 – Weight loss of samples with M in different temperature ranges associated with the three zones for chloride-free and chloride-containing mixtures.

T^e °C range/associated weight loss	M %loss	MO %loss	MA %loss	MC %loss	MOC %loss	MAC %loss
105–250/(C—S—H, C—(A)—S—H) gels water	9.03	6.14	5.50	4.64	4.21	3.85
250–400/water in Friedel's salt	–	–	–	3.07	2.04	1.12
400–550/dehydration of Portlandite	0.87	0.67	1.79	2.08	3.17	1.69
550–1100 (carbonates)	0.68	0.56	0.86	5.20	5.36	4.69
(550–1100) × 0.41 (carbonated portlandite)	0.28	0.23	0.35	2.13	2.20	1.92

tain in samples with G is approximately 2.7 times higher than in blends with M.

In relation to the effect of nanosilica in the carbonation process of M and G, carbonation process is different according to observed in the graphs. Weight loss associated to carbonates release as CO_2 for samples with metakaolin takes place around 750–950 °C and between 850 and 1100 °C for samples with G according to Figs. 3 and 4. The addition of chlorides favour that blends release carbonates displaced or substituted by chlorides to form Friedel salts in samples with and without nanosilica. The signal at approximately 170 °C could indicate the formation of Strantlingite [70] as was clearly observed as individual band in samples without nanosilica (M, G) or with nanosilica OX (GO) or overlapped in samples MO, MA and GA.

From a more general perspective, in view of these results it can be said that the addition of nanosilica has shown a negative influence in the M blends compared to the G blends with regard to the ability to generate C—S—H and C—(A)—S—H gels such as the chlorides addition negatively affects to gel formation, being more significant for blends with M than for G ones and more for reference samples without nanosilica added. Apparently, the incorporation of Al into the C—A—S—H gel could lead to an increase of bound water in the gel [59], however it has been observed throughout this experimental study that this water is a consequence of the effect of the nanosilica in the case of samples with G not so in M ones. It has also been observed that G shows a higher tendency to form CAH hydration products or carbonates [40,49]. A quantification of the mass fraction of the Friedel's salt (mFS (wt.%)) can be calculated by Eq. (1) [13,68,69] in order to estimate which addition has the highest Friedel's salt formation capacity and thereafter compare the results by DTG and other techniques.

$$\mathrm{mFS\,(wt.\%)} = \left(\frac{\mathrm{MFS}}{6\mathrm{MH_2O}}\right) \times \mathrm{mH_2O} \quad (1)$$

where MFS is the molecular weight of Friedel's salt (561.3 g/mol), MH_2O is the molecular weight of water (18.02 g/mol) and mH_2O is the TGA mass loss for Friedel's salt water at the peak in the range (250–400 °C) [13,21] in the DTG curve. The values calculated by Eq. (1) are shown in Table 6 for weight losses associated to Friedel's salt in the range 250–400 °C for samples exposed to chlorides, according to Figs. 3 and 4.

Al_2O_3 contain is related to FS formation and to carry out the comparison between the capacity of formation of M and G such as the influence of nanosilica addition in the chemically bound of Cl^- all the blends have the same Al_2O_3 contain. Table 6 shows that the formation of Friedel's salt (FS) have the same tendency that C—S—H and C—(A)—S—H gels formation, where the addition of nanosilica to metakaolin decrease the FS formation being this behaviour opposite for blends with G, in which nanosilica addition favour FS formation. Point to the similar FS formation capacity between M and G reference samples. To combine chemically chlorides by FS formation is slightly better use lower surface nanosilica O.

From the results obtained by the techniques previously described such XRD and FTIR, very few Friedel's salt or none was observed in the GC, GOC and GAC samples, hence this water loss could be associated to another type of combination, such as physisorption in the interlayers of the C—S—H gel [26,28,64] although DTA–TG analysis has allowed quantify FS formation according to literature. Hydrocalcite could be included in this loss since the range of loss lies between 300 and 400 °C [55,56]. In XRD the typical Hydrocalcite peaks could be observed for samples with G, so this could be a logical explanation for this case.

Chlorides contain determined by potentiometric titration with $AgNO_3$

Numerous previous works show the presence of combined chlorides at different depths from the exposed surface of virtually any type of concrete. In this work the free interaction of combinations of M and G with nanosilica was promoted to observe the reaction of this additions in a $Ca(OH)_2$ saturated medium and incorporating Cl^- in a controlled environment. In this experimental study the volume of total, free and combined chlorides generated with each pozzolanic addition and blends have been measured. As a novel contribution, in this work the combined chlorides are quantified, distinguishing those chemically combined as Friedel's salt from those phys-

Table 6 – Quantification by DTA–TG analysis of Friedel's salt (FS) formed in a temperature range between 250 and 400 °C and chlorides chemically combined contained in FS.

	M-C	M-O-C	M-A-Cl	G-Cl	G-O-C	G-A-C
wt% loss (water in Friedel's salt)	3.114	1.836	1.117	2.862	4.156	3.999
Moles FS	0.02839	0.01698	0.010335	0.026477	0.038445	0.03699
wt.% Cl^- chemically combined in FS	**2.04192**	**1.2043**	**0.73279**	**1.87726**	**2.72576**	**2.62268**

Table 7 – Total, free and combined chlorides in the mixtures prepared with M and G alone and with both nanosilica after 21 days in agitation.

Sample	Total Cl^- (wt.%)	Free Cl^- (wt.%)	% of free Cl	Combined Cl wt.% (FS and physisorbed in gel C—S—H and C—(A)—S—H) = total Cl–free Cl	% of combined Cl	Rate combined Cl/free Cl
MC	5.76	2.18	37.85	**3.58**	62.15	1.64
MOC	5.44	2.47	45.40	**2.97**	54.60	1.20
MAC	6.28	3.32	52.87	**2.96**	47.13	0.89
GC	3.90	1.47	37.69	**2.43**	62.31	1.65
GOC	5.41	2.73	50.46	**2.68**	49.54	0.98
GAC	6.00	3.17	49.35	**3.00**	50.65	1.03

ically combined, physisorbed in the C—S—H or C—(A)—S—H gel, since there are very few previous works that have studied so. This experimental results could be of great interest to assess which addition and combination would present a greater potential for the generation of free chlorides that can induce corrosion of concrete reinforcement. Furthermore, these results can also provide valuable information about the combining capacity and its stability against environmental phenomena such as carbonation, of the additions studied.

Table 7 shows the results for total, free and combined chlorides obtained by potentiometric titration with $AgNO_3$. The presence of combined chlorides should not pose a risk for corrosion in reinforced concrete, since they are not free to react. Among the combined chlorides can be distinguished between those physisorbed in gels and those chemically bound, particularly as Friedel's salt, the latter being more stable. The MAC and GAC samples have the highest percentage of total Cl^- while the GC shows the lowest amount of total Cl^- in percentage. Free Cl^- values showed a very similar trend to the total Cl^- values. When homogenising the results in percentage amounts with respect to the mass of total Cl^-, it is observed that the percentage of free chloride is practically the same for MC and GC samples. Combined chlorides in Friedel's salt and physisorbed in C—S—H and C—(A)—S—H show the same tendency that the results obtained in the DTA–TG analysis. For blends with M, chloride binding capacity decrease with the addition of nanosilica and for samples with G the combined chlorides is greater for samples with nanosilica than for one without it. It is important point to that both samples without nanosilica (M and G) show the highest % of combined chlorides and the highest rate combined chlorides vs free chlorides. Free chlorides, the type that can cause a corrosion problem, are identical in wt.% for both M and G blends and increase slightly up to 50 wt.%, when nanosilica is added in both additions.

Once the combined chlorides are obtained from the potentiometric titration, the comparison quantification of chlorides in the Friedel's salt obtained by ATD–TG and titration is carried out.

As is well known, given the free chloride values, the percentage of combined Cl^- can be estimated by the difference between total and free chlorides. The result obtained would apparently indicate that both pozzolanic additions without nanosilica have similar capacity of FS formation. The comparison between combined chlorides determined by potentiometric titration and FS quantified by DTA–TG indicates that both analysis techniques are in agreement. The trend between combined chlorides determined by titration and Cl^- bounds in FS, quantified by DTA–TG analysis are in agreement when nanosilica is added, being this tendency opposite, increasing for samples with G and decreasing for M blends. However, when these results were confronted with techniques of semiquantitative analysis such XRD and FTIR, the chemical combinations similar to Friedel's salt have only been verified in the case of MC sample. Combined chlorides in FS for samples with M clearly tend to decrease when nanosilica is incorporated: 57 wt.% of the Cl^- corresponds to Friedel's salt in the MC sample, 40% in the MOC and 24 wt.% in the MAC. The level of Cl^- physisorption is high for the M but the presence of Friedel's salt is evidence of the chloride's ability to form a stable structure, retaining chlorides, improving the resistance to Cl^- penetration in concrete. Unlike the samples with M, blends with G increases combined chlorides in FS and this increase is maintained even for samples that contain NS: 77 wt.% of the Cl^- corresponds to Friedel's salt in the GC sample, 100% in the GOC and 87 wt.% in the GAC. Compared to M blends, in samples with G the level of Cl^- physisorption is low showing that G has a very high capacity to form Friedel's salt, a stable crystalline structure that bound Cl^- in a structure, retaining them, improving the resistance to penetration

Table 8 – Quantification of combined chlorides, chemically combined in FS and physisorbed in C—S—H and C—(A)—S—H gels for mixtures with M and G according to Cl^- combined determined by potentiometric titration and Cl^- in Friedel's salt quantified by DTA–TG analysis.

	Wt.% combined Cl^-	Wt.% Cl^- in Friedel's salt (% of combined Cl^-)	Wt.% physisorbed Cl^- (% of combined Cl^-)
MC	3.58	2.04 (56.98)	1.54 (43.01)
MOC	2.97	1.20 (40.40)	1.77 (59.60)
MAC	2.96	0.73 (24.66)	2.23 (75.34)
GC	2.43	1.87 (76.95)	0.56 (23.05)
GOC	2.68	2.72 (100)	−0.04
GAC	3.00	2.62 (87.33)	0.38 (12.64)

in concrete. All these effects translate into improvements in performance and durability that could be promising for these combinations.

As can be seen in Table 8, NS plays an antagonistic role with M as the O and A additions reduce Friedel's salt formation by 17 and 32% respectively and a synergistic effect in chemical Cl^- combination in blends with G and nanosilica with increases of 23 and 12% for the addition of O and A respectively.

Conclusions

This research was carried out with a future goal of decreasing the rate of Portland cement production and generating a positive environmental impact by promoting the use of SMCs to improve the lifetime of structures exposed to aggressive agents such as chlorides. The chloride binding capacity of mixtures with sustainable additions such as M and G was assessed according to their origin. Blends were designed with different amounts of M and G but with a constant Al_2O_3 contain, involved in the chemical Cl^- combination by formation of Friedel's salt to which two types of nanosilica with different specific surface areas in an aqueous phase saturated in calcium hydroxide. The following conclusions can be drawn:

- The DTA–TG analysis is a very useful tool for quantify hydration products such as C—S—H and C—(A)—S—H gels, portlandite and results as an essential, simple and available technique, complementary to XRD semiquantitative analysis, to determine the chemical combination capacity of chlorides by quantifying the formation of Friedel's salt ($3CaO\,Al_2O_3{\cdot}CaCl_2{\cdot}10H_2O$).
- Nanosilica addition to samples with M and G regardless of the specific surface decreases gels C—S—H and C—(A)—S—H formation, more noticeably for samples with M.
- According to total chlorides determined by potentiometric titration and chemically combined chlorides contained in the Friedel's salt by DTA–TG analysis it is possible to estimate physisorbed chlorides in C—S—H and C—(A)—S—H gels by the difference between both amounts.
- M compared to G has shown higher physisorbed chlorides combination capacity in gels although the capacity of Friedel's salt formation (chemical binding) is very high for both pozzolanic SCMs.
- Nanosilica addition to M, regardless nanosilica specific surface, decreases Friedel's salt formation capacity, being this trend opposite to what happens when chlorides are added to blends with G and nanosilica.
- Chlorides addition meaningfully replaces carbonates in carboaluminates phases to form Friedel's salt, being this exchange higher for samples with M than for G blends.

This result is very valuable for the design of Portland cement base materials, the high chloride binding capacity of M and G sustainable pozzolanic additions in agreement to the high Friedel's salt formation capacity related with a high durability behaviour against a very important aggressive agents such is chloride. In contrast, nanosilica limit the ability of M to combine chlorides, which is associated with the high specific surface area of NS and the different Al_2O_3 structure although it is demonstrated that this pozzolanic nanoaddition improve the pore refinement or densification of the microstructure. M is actually a very important SCM material used to design sustainable cement based materials decreasing the clinker contain such as LC^3 (limestone calcined clay cement) and therefore reducing CO_2 emissions.

Conflict of interest

The authors declare that there is no conflict of interest regarding the publication of this paper.

Acknowledgements

This work was supported by the Spanish Ministry of Science and Innovation and FEDER funds (EU) through the Project RTI2018-100962-B-I00: Sustainable strategy of high durability in concretes exposed to marine environment at early ages (ESDUHOTE), Project TED2021-130734B-I00 titled: "Nanotechnology as durability strategy in sustainable cements" (VERNADUR) Ecological Transition and Digital Transition Projects (2021), Project PID2021-128616OB-I00 titled: Design of nanostructured concretes with reduced Portland cement content and high durability from an early age as an effective strategy towards sustainability (DIHORNARE) Knowledge Generation Projects.

REFERENCES

[1] E. Gartner, Industrially interesting approaches to "low-CO_2" cements, Cem. Concr. Res. 34 (2004) 1489–1498, http://dx.doi.org/10.1016/j.cemconres.2004.01.021.
[2] M.G. Stewart, X. Wang, M.N. Nguyen, Climate change adaptation for corrosion control of concrete infrastructure,

Struct. Saf. 35 (2012) 29–39, http://dx.doi.org/10.1016/j.strusafe.2011.10.002.
[3] P. Schiessl, Durability of reinforced concrete structures, Constr. Build. Mater. 10 (1996) 289–292, http://dx.doi.org/10.1016/0950-0618(95)00072-0.
[4] F. Qu, W. Li, W. Dong, V.W.Y. Tam, T. Yu, Durability deterioration of concrete under marine environment from material to structure: a critical review, J. Build. Eng. 35 (2021) 102074, http://dx.doi.org/10.1016/j.jobe.2020.102074.
[5] Q. Yuan, C. Shi, G. De Schutter, K. Audenaert, D. Deng, Chloride binding of cement-based materials subjected to external chloride environment – a review, Constr. Build. Mater. 23 (2009) 1–13, http://dx.doi.org/10.1016/j.conbuildmat.2008.02.004.
[6] M. Zahedi, A.A. Ramezanianpour, A.M. Ramezanianpour, Evaluation of the mechanical properties and durability of cement mortars containing nanosilica and rice husk ash under chloride ion penetration, Constr. Build. Mater. 78 (2015) 354–361, http://dx.doi.org/10.1016/j.conbuildmat.2015.01.045.
[7] A. Pilvar, A.A. Ramezanianpour, H. Rajaie, New method development for evaluation concrete chloride ion permeability, Constr. Build. Mater. 93 (2015) 790–797, http://dx.doi.org/10.1016/j.conbuildmat.2015.05.092.
[8] H.-W. Song, C.-H. Lee, K.Y. Ann, Factors influencing chloride transport in concrete structures exposed to marine environments, Cem. Concr. Compos. 30 (2008) 113–121, http://dx.doi.org/10.1016/j.cemconcomp.2007.09.005.
[9] Chloride-induced corrosion, in: Corrosion of Steel in Concrete, 2003: pp. 91–108. https://doi.org/10.1002/3527603379.ch6.
[10] I. Galan, F.P. Glasser, Chloride in cement, Adv. Cem. Res. 27 (2015) 63–97, http://dx.doi.org/10.1680/adcr.13.00067.
[11] R. Lannegrand, G. Ramos, R. Talero, Estado del conocimiento sobre la sal de Friedel, Mater. Constr. 51 (2001) 63–71, http://dx.doi.org/10.3989/mc.2001.v51.i262.372.
[12] Z. Shi, M.R. Geiker, K. De Weerdt, T.A. Østnor, B. Lothenbach, F. Winnefeld, J. Skibsted, Role of calcium on chloride binding in hydrated Portland cement–metakaolin–limestone blends, Cem. Concr. Res. 95 (2017), http://dx.doi.org/10.1016/J.CEMCONRES.201702003.
[13] Z. Shi, M.R. Geiker, B. Lothenbach, K. De Weerdt, S.F. Garzón, K. Enemark-Rasmussen, J. Skibsted, Friedel's salt profiles from thermogravimetric analysis and thermodynamic modelling of Portland cement-based mortars exposed to sodium chloride solution, Cem. Concr. Compos. 78 (2017) 73–83, http://dx.doi.org/10.1016/j.cemconcomp.2017.01.002.
[14] R. Loser, B. Lothenbach, A. Leemann, M. Tuchschmid, Chloride resistance of concrete and its binding capacity – comparison between experimental results and thermodynamic modeling, Cem. Concr. Compos. 32 (2010) 34–42, http://dx.doi.org/10.1016/j.cemconcomp.2009.08.001.
[15] A.R. Bagheri, H. Zanganeh, Comparison of rapid tests for evaluation of chloride resistance of concretes with supplementary cementitious materials, J. Mater. Civ. Eng. 24 (2012) 1175–1182, http://dx.doi.org/10.1061/(ASCE)MT.1943-5533.0000485.
[16] C. Meyer, The greening of the concrete industry, Cem. Concr. Compos. 31 (2009) 601–605, http://dx.doi.org/10.1016/j.cemconcomp.2008.12.010.
[17] K.L. Scrivener, V.M. John, E.M. Gartner, Eco-efficient cements: potential economically viable solutions for a low-CO_2 cement-based materials industry, Cem. Concr. Res. 114 (2018) 2–26, http://dx.doi.org/10.1016/j.cemconres.2018.03.015.
[18] J.O. Ighalo, A.G. Adeniyi, A perspective on environmental sustainability in the cement industry, Waste Dispos. Sustain. Energy 2 (2020) 161–164, http://dx.doi.org/10.1007/s42768-020-00043-y.
[19] M. Valipour, F. Pargar, M. Shekarchi, S. Khani, Comparing a natural pozzolan, zeolite, to metakaolin and silica fume in terms of their effect on the durability characteristics of concrete: a laboratory study, Constr. Build. Mater. 41 (2013) 879–888, http://dx.doi.org/10.1016/j.conbuildmat.2012.11.054.
[20] K. De Weerdt, A. Colombo, L. Coppola, H. Justnes, M.R. Geiker, Impact of the associated cation on chloride binding of Portland cement paste, Cem. Concr. Res. 68 (2015) 196–202, http://dx.doi.org/10.1016/j.cemconres.2014.01.027.
[21] F. Qu, W. Li, Y. Guo, S. Zhang, J.L. Zhou, K. Wang, Chloride-binding capacity of cement-GBFS-nanosilica composites under seawater chloride-rich environment, Constr. Build. Mater. 342 (2022) 127890, http://dx.doi.org/10.1016/j.conbuildmat.2022.127890.
[22] A. Cheng, R. Huang, J.-K. Wu, C.-H. Chen, Influence of GGBS on durability and corrosion behavior of reinforced concrete, Mater. Chem. Phys. 93 (2005) 404–411, http://dx.doi.org/10.1016/j.matchemphys.2005.03.043.
[23] R. García, E. Reyes, P. Villanueva, M.Á. de la Rubia, J. Fernández, A. Moragues, Service life and early age durability enhancement due to combined metakaolin and nanosilica in mortars for marine applications, Materials 13 (2020) 1169, http://dx.doi.org/10.3390/ma13051169.
[24] J. Björnström, A. Martinelli, A. Matic, L. Börjesson, I. Panas, Accelerating effects of colloidal nano-silica for beneficial calcium–silicate–hydrate formation in cement, Chem. Phys. Lett. 392 (2004) 242–248, http://dx.doi.org/10.1016/j.cplett.2004.05.071.
[25] B. Lothenbach, A. Nonat, Calcium silicate hydrates: solid and liquid phase composition, Cem. Concr. Res. 78 (2015) 57–70, http://dx.doi.org/10.1016/j.cemconres.2015.03.019.
[26] G. Plusquellec, A. Nonat, Interactions between calcium silicate hydrate (C–S–H) and calcium chloride, bromide and nitrate, Cem. Concr. Res. 90 (2016) 89–96, http://dx.doi.org/10.1016/j.cemconres.2016.08.002.
[27] J.J. Beaudoin, V.S. Ramachandran, R.F. Feldman, Interaction of chloride and C–S–H, Cem. Concr. Res. 20 (1990) 875–883, http://dx.doi.org/10.1016/0008-8846(90)90049-4.
[28] D. Hou, Y. Jia, J. Yu, P. Wang, Q. Liu, Transport properties of sulfate and chloride ions confined between calcium silicate hydrate surfaces: a molecular dynamics study, J. Phys. Chem. C 122 (2018) 28021–28032, http://dx.doi.org/10.1021/acs.jpcc.8b07484.
[29] G. Plusquellec, I. Pochard, A. Nonat, Anion uptake by calcium silicate hydrate, 2012.
[30] V.S. Ramachandran, Possible states of chloride in the hydration of tricalcium silicate in the presence of calcium chloride, Matér. Constr. 4 (1971) 3–12, http://dx.doi.org/10.1007/BF02473926.
[31] T. Luping, L.-O. Nilsson, Chloride binding capacity and binding isotherms of OPC pastes and mortars, Cem. Concr. Res. 23 (1993) 247–253, http://dx.doi.org/10.1016/0008-8846(93)90089-R.
[32] H. Zibara, R.D. Hooton, M.D.A. Thomas, K. Stanish, Influence of the C/S and C/A ratios of hydration products on the chloride ion binding capacity of lime-SF and lime-MK mixtures, Cem. Concr. Res. 38 (2008) 422–426, http://dx.doi.org/10.1016/j.cemconres.2007.08.024.
[33] J.I. Tobón, J. Payá, O.J. Restrepo, Study of durability of Portland cement mortars blended with silica nanoparticles, Constr. Build. Mater. 80 (2015) 92–97, http://dx.doi.org/10.1016/j.conbuildmat.2014.12.074.
[34] M. Stefanidou, I. Papayianni, Influence of nano-SiO_2 on the Portland cement pastes, Compos. Part B: Eng. 43 (2012) 2706–2710, http://dx.doi.org/10.1016/j.compositesb.2011.12.015.
[35] M. Gesoğlu, E. Güneyisi, T. Özturan, K. Mermerdaş, Permeability properties of concretes with high reactivity

metakaolin and calcined impure kaolin, Mater. Struct. 47 (2014) 709–728, http://dx.doi.org/10.1617/s11527-013-0090-9.
[36] B.B. Sabir, S. Wild, J. Bai, Metakaolin and calcined clays as pozzolans for concrete: a review, Cem. Concr. Compos. 23 (2001) 441–454, http://dx.doi.org/10.1016/S0958-9465(00)00092-5.
[37] P. Dinakar, S.N. Manu, Concrete mix design for high strength self-compacting concrete using metakaolin, Mater. Des. 60 (2014) 661–668, http://dx.doi.org/10.1016/j.matdes.2014.03.053.
[38] J. Ambroise, S. Maximilien, J. Pera, Properties of Metakaolin blended cements, Adv. Cem. Based Mater. 1 (1994) 161–168, http://dx.doi.org/10.1016/1065-7355(94)90007-8.
[39] A.K. Parande, B. Ramesh Babu, M. Aswin Karthik, K.K. Deepak Kumaar, N. Palaniswamy, Study on strength and corrosion performance for steel embedded in metakaolin blended concrete/mortar, Constr. Build. Mater. 22 (2008) 127–134, http://dx.doi.org/10.1016/j.conbuildmat.2006.10.003.
[40] R.K. Dhir, M.A.K. El-Mohr, T.D. Dyer, Chloride binding in GGBS concrete, Cem. Concr. Res. 26 (1996) 1767–1773, http://dx.doi.org/10.1016/S0008-8846(96)00180-9.
[41] R. El Shazly, Effect of Slag as a Fine Aggregate on Mechanical, Corrosion, and Nuclear Attenuation Properties of Concrete, 2017.
[42] İ.B. Topçu, A.R. Boğa, Effect of ground granulate blast-furnace slag on corrosion performance of steel embedded in concrete, Mater. Des. 31 (2010) 3358–3365, http://dx.doi.org/10.1016/j.matdes.2010.01.057.
[43] R. Luo, Y. Cai, C. Wang, X. Huang, Study of chloride binding and diffusion in GGBS concrete, Cem. Concr. Res. 7 (2003).
[44] J.-Y. Shih, T.-P. Chang, T.-C. Hsiao, Effect of nanosilica on characterization of Portland cement composite, Mater. Sci. Eng. A 424 (2006) 266–274, http://dx.doi.org/10.1016/j.msea.2006.03.010.
[45] D. da Silva Andrade, J.H. da Silva Rêgo, P.C. Morais, A.N. de Mendonça Lopes, M.F. Rojas, Investigation of C–S–H in ternary cement pastes containing nanosilica and highly-reactive supplementary cementitious materials (SCMs): microstructure and strength, Constr. Build. Mater. 198 (2019) 445–455, http://dx.doi.org/10.1016/j.conbuildmat.2018.10.235.
[46] R. Garcia, M.A. de la Rubia, E. Enriquez, A. del Campo, J. Fernandez, A. Moragues, Chloride binding capacity of metakaolin and nanosilica supplementary pozzolanic cementitious materials in aqueous phase, Constr. Build. Mater. 298 (2021) 123903, http://dx.doi.org/10.1016/j.conbuildmat.2021.123903.
[47] A.K. Suryavanshi, J.D. Scantlebury, S.B. Lyon, Mechanism of Friedel's salt formation in cements rich in tri-calcium aluminate, Cem. Concr. Res. 26 (1996) 717–727, http://dx.doi.org/10.1016/S0008-8846(96)85009-5.
[48] A.M. Aguirre-Guerrero, R. Mejia, Durabilidad del hormigón armado expuesto a condiciones agresivas, Mater. Constr. 63 (2013) 7–38, http://dx.doi.org/10.3989/mc.2013.00313.
[49] Z. Yang, S. Sui, L. Wang, T. Feng, Y. Gao, S. Mu, L. Tang, J. Jiang, Improving the chloride binding capacity of cement paste by adding nano-Al_2O_3: the cases of blended cement pastes, Constr. Build. Mater. 232 (2020) 117219, http://dx.doi.org/10.1016/j.conbuildmat.2019.117219.
[50] E.G. Badogiannis, I.P. Sfikas, D.V. Voukia, K.G. Trezos, S.G. Tsivilis, Durability of metakaolin self-compacting concrete, Constr. Build. Mater. 82 (2015) 133–141, http://dx.doi.org/10.1016/j.conbuildmat.2015.02.023.
[51] P. Duan, Z. Shui, W. Chen, C. Shen, Effects of metakaolin, silica fume and slag on pore structure, interfacial transition zone and compressive strength of concrete, Constr. Build. Mater. 44 (2013) 1–6, http://dx.doi.org/10.1016/j.conbuildmat.2013.02.075.
[52] R. Garcia, N. Henao, M.A. De la Rubia, A. Moragues, J. Fernandez, Early contributing nanostructured cementitious matrix designs: benefits in durable features at early ages, Constr. Build. Mater. 241 (2020) 117941, http://dx.doi.org/10.1016/j.conbuildmat.2019.117941.
[53] A. Ipavec, R. Gabrovšek, T. Vuk, V. Kaučič, J. Maček, A. Meden, Carboaluminate phases formation during the hydration of calcite-containing portland cement: carboaluminate phase formation, J. Am. Ceram. Soc. 94 (2011) 1238–1242, http://dx.doi.org/10.1111/j.1551-2916.2010.04201.x.
[54] W. Deboucha, N. Sebaibi, Y. El Mendili, A. Fabien, U.J. Alengaram, N. Leklou, M.N. Hamdadou, A. Bourdot, S. Gascoin, Reactivity effect of calcium carbonate on the formation of carboaluminate phases in ground granulated blast furnace slag blended cements, Sustainability 13 (2021) 6504, http://dx.doi.org/10.3390/su13116504.
[55] O. Kayali, M.S.H. Khan, M. Sharfuddin Ahmed, The role of hydrotalcite in chloride binding and corrosion protection in concretes with ground granulated blast furnace slag, Cem. Concr. Compos. 34 (2012) 936–945, http://dx.doi.org/10.1016/j.cemconcomp.2012.04.009.
[56] A. Machner, M. Zajac, M. Ben Haha, K.O. Kjellsen, M.R. Geiker, K. De Weerdt, Chloride-binding capacity of hydrotalcite in cement pastes containing dolomite and metakaolin, Cem. Concr. Res. 107 (2018) 163–181, http://dx.doi.org/10.1016/j.cemconres.2018.02.002.
[57] Y. Zhang, O. Çopuroğlu, Role of the grain size on the hydration characteristics of slag in an aged field concrete, Cem. Concr. Res. 162 (2022) 106985, http://dx.doi.org/10.1016/j.cemconres.2022.106985.
[58] S. Grangeon, F. Claret, C. Roosz, T. Sato, S. Gaboreau, Y. Linard, Structure of nanocrystalline calcium silicate hydrates: insights from X-ray diffraction, synchrotron X-ray absorption and nuclear magnetic resonance, J. Appl. Crystallogr. 49 (2016) 771–783, http://dx.doi.org/10.1107/S1600576716003885.
[59] E. Kapeluszna, Ł. Kotwica, A. Różycka, Ł. Gołek, Incorporation of Al in C–A–S–H gels with various Ca/Si and Al/Si ratio: microstructural and structural characteristics with DTA/TG, XRD, FTIR and TEM analysis, Constr. Build. Mater. 155 (2017) 643–653, http://dx.doi.org/10.1016/j.conbuildmat.2017.08.091.
[60] I.G. Richardson, A.R. Brough, R. Brydson, G.W. Groves, C.M. Dobson, Location of aluminum in substituted calcium silicate hydrate (C–S–H) gels as determined by 29Si and 27Al NMR and EELS, J. Am. Ceram. Soc. 76 (1993) 2285–2288, http://dx.doi.org/10.1111/j.1151-2916.1993.tb07765.x.
[61] R.J. Myers, S.A. Bernal, J.D. Gehman, J.S.J. van Deventer, J.L. Provis, The role of Al in cross-linking of alkali-activated slag cements, J. Am. Ceram. Soc. 98 (2015) 996–1004, http://dx.doi.org/10.1111/jace.13360.
[62] S.A. Hosseini, A. Niaei, D. Salari, Production of γ-Al_2O_3 from kaolin, OJPC 01 (2011) 23–27, http://dx.doi.org/10.4236/ojpc.2011.12004.
[63] I.F. Sáez del Bosque, Modificaciones nanoestructurales en pastas de cemento [Doctoral], Universidad Autónoma de Madrid Instituto de Ciencias de la Construcción Eduardo Torroja, 2012.
[64] R. García, M. Ángel de la Rubia, J. Fernández, P. Villanueva, A. Moragues, Effect of carbonation in high chloride-binding capacity mortars subjected to a marine environment at early ages, J. Build. Eng. 40 (2021) 102355, http://dx.doi.org/10.1016/j.jobe.2021.102355.
[65] V.S. Ramachandran, R.F. Feldman, P.J. Sereda, Application of differential thermal analysis in cement research. Research on aggregate, cement, concrete and epoxy bonding, Highway Research Board. 62 (1964) 40–61.
[66] X. Gaviria, M.V. Borrachero, J. Payá, J.M. Monzó, J.I. Tobón, Mineralogical evolution of cement pastes at early ages based

on thermogravimetric analysis (TG), J. Therm. Anal. Calorim. 132 (2018) 39–46, http://dx.doi.org/10.1007/s10973-017-6905-0.
[67] H. Chang, Chloride binding capacity of pastes influenced by carbonation under three conditions, Cem. Concr. Compos. 84 (2017) 1–9, http://dx.doi.org/10.1016/j.cemconcomp.2017.08.011.
[68] Y. Zheng, M. Russell, G. Davis, D. McPolin, K. Yang, P.A.M. Basheer, S. Nanukuttan, Influence of carbonation on the bound chloride concentration in different cementitious systems, Constr. Build. Mater. 302 (2021) 124171, http://dx.doi.org/10.1016/j.conbuildmat.2021.1241.71.
[69] B. Guo, G. Qiao, P. Han, Z. Li, Q. Fu, Effect of natural carbonation on chloride binding behaviours in OPC paste investigated by a thermodynamic model, J. Build. Eng. 49 (2022) 104021, http://dx.doi.org/10.1016/j.jobe.2022.104021.
[70] S. Kwan, J. LaRosa, M.W. Grutzeck, 29Si and 27Al MASNMR study of stratlingite, J. Am. Ceram. Soc. 78 (1995) 1921–1926, http://dx.doi.org/10.1111/j.1151-2916.1995.tb08910.x.